Hindawi
Journal of Chemistry
Volume 2024, Article ID 5084553, 19 pages
https://doi.org/10.1155/2024/5084553

Research Article

Multistaged *In Silico* Discovery of the Best SARS-CoV-2 Main Protease Inhibitors amongst 3009 Clinical and FDA-Approved Compounds

Ibrahim H. Eissa,[1] **Abdulrahman M. Saleh**,[1] **Sara T. Al-Rashood**,[2] **Abdul-Aziz M. M. El-Attar**,[3] **and Ahmed M. Metwaly**[4,5]

[1]*Pharmaceutical Medicinal Chemistry & Drug Design Department, Faculty of Pharmacy (Boys), Al-Azhar University, Cairo 11884, Egypt*
[2]*Department of Pharmaceutical Chemistry, College of Pharmacy, King Saud University, P.O. Box 2457, Riyadh 11451, Saudi Arabia*
[3]*Pharmaceutical Analytical Chemistry Department, Faculty of Pharmacy, Al-Azhar University, Cairo 11884, Egypt*
[4]*Pharmacognosy and Medicinal Plants Department, Faculty of Pharmacy (Boys), Al-Azhar University, Cairo 11884, Egypt*
[5]*Biopharmaceutical Products Research Department, Genetic Engineering and Biotechnology Research Institute, City of Scientific Research and Technological Applications (SRTA-City), Alexandria 21934, Egypt*

Correspondence should be addressed to Ibrahim H. Eissa; ibrahimeissa@azhar.edu.eg and Ahmed M. Metwaly; ametwaly@azhar.edu.eg

Received 16 March 2022; Revised 9 February 2024; Accepted 10 February 2024; Published 6 March 2024

Academic Editor: Andrea Penoni

Copyright © 2024 Ibrahim H. Eissa et al. This is an open access article distributed under the Creative Commons Attribution License, which permits unrestricted use, distribution, and reproduction in any medium, provided the original work is properly cited.

As a follow-up to our teamwork's former work against SARS-CoV-2, eight compounds (ramelteon (**68**), prilocaine (**224**), nefiracetam (**339**), cyclandelate (**911**), mepivacaine (**2325**), ropivacaine (**2351**), tasimelteon (**2384**), and levobupivacaine (**2840**)) were revealed as the best potentially active SARS-CoV-2 inhibitors targeting the main protease (PDB ID: 5R84), M^{pro}. The compounds were named in the midst of 3009 FDA and clinically approved compounds employing a multistaged *in silico* method. A molecular fingerprints study with **GWS**, the cocrystallized ligand of the M^{pro}, indicated the resemblance of 150 candidates. Consequently, a structure similarity experiment disclosed the best twenty-nine analogous. Then, molecular docking studies were done against the M^{pro} active site and showed the binding of the best compounds. Next, a 3D-pharmacophore study confirmed the obtained results for the eight compounds by exhibiting relative fit values of more than 90% (except for **68**, 74%, and **2384**, 83%). Levobupivacaine (**2840**) showed the most accurate docking and pharmacophore scores and was picked for further MD simulations experiments (RMSD, RMSF, R_g, SASA, and H-H bonding) over 100 ns. The MD simulations results revealed the accurate binding as well as the optimum dynamics of the M^{pro}-levobupivacaine complex. Finally, MM-PBSA studies were conducted and indicated the favorable bonding of the M^{pro}-levobupivacaine complex with a free energy value of −235 kJ/mol. The fulfilled outcomes hold out hope of beating COVID-19 through more *in vitro* and *in vivo* research for the named compounds.

1. Introduction

The WHO noted on March 4, 2022, that the confirmed infections of COVID-19 on a worldwide basis are 440,807,756 humans. In sorrow, 5,978,096 humans among them are dead [1]. Despite the fact that the number of vaccine doses reached 10,585,766,316, the dangerous virus still has the ability to infect vastly [2]. According to these horrible numbers, massive work is demanded from scientists all over the world to find a cure. The routine process of drug discovery and detection is greatly expensive and lasts for a very long time. The usual time needed for new drug discovery is twelve years costing about 2.6 billion USD [3]. On the other hand, drug repurposing is a much faster process [4, 5].

Drug repurposing includes the identification of new biological use or uses for an old drug [6]. The process of drug repositioning was employed successfully in the development of anticancer [7], anti-COVID-19 [8], anti-inflammatory [9] antibacterial [10], antiparasitic [11], and antiviral [12] drugs.

Methods of computational chemistry were used to explore various pharmacokinetic and pharmacodynamic parameters that connect the chemical structure to activity as well as to explore the interaction of ligands with biological proteins such as structure similarity [13], molecular fingerprints [14], QSAR [15], pharmacophores [16], homology models [17], molecular modeling, drug molecular design [18], rational drug design [19], molecular docking [20], MD simulations [21], absorption [22], distribution, metabolism [23], excretion [24], and toxicity properties [25] as well as physicochemical characterization [26] assessment and DFT.

For that reason, our team composed a multiple-phase computational screening approach to name the most effective inhibitor/s for an essential SARS-CoV-2 enzyme in the midst of hundreds or thousands of compounds. Among a set of 310 antiviral natural metabolites, we pointed the most potential inhibitors against various SARS-CoV-2 proteins, including nsp10 [27], helicase [28], the main protease [29, 30], and the papain-like protease [31]. Similarly, the most potential FDA-approved drugs were anticipated against the SARS-CoV-2 nsp16-nsp10 2′-o-methyltransferase complex [32] and the SARS-CoV-2 RNA-dependent RNA polymerase [33]. We also expected potential natural inhibitors for the SARS-CoV-2 helicase [34] and RdRp [35].

Viral proteases stand out as promising targets for the development of antiviral treatments, demonstrating efficacy against specific viruses such as the human immunodeficiency virus and hepatitis C virus when targeted by aspartyl and serine proteases, respectively [36]. In the context of SARS-CoV-2, the main protease (M^{pro}) plays a pivotal role in the activation of sixteen functional and nonstructural proteins through the cleavage of the large polyproteins (pp1a and pp1ab). The inhibition of M^{pro} emerges as a strategic approach, causing substantial impairment to the virus and impeding its replication [37]. It is noteworthy that the structural and sequential distinctions between the viral main protease (M^{pro}) and human proteases further emphasize M^{pro} as a viable target for anti-COVID-19 drug discovery [38]. The unique structural properties of the SARS-CoV-2 M^{pro}, coupled with its significant role in the viral life cycle, underscore its potential as a focal point for developing novel and effective therapeutic interventions against COVID-19 [39, 40]. In this work, a set of 3009 clinical and FDA-approved compounds were retrieved from the website of https://Selleckchem.com [41] and has been subjected to multi-staged *in silico* methods to determine the most potent inhibitors targeting SARS-CoV-2 main protease (M^{pro}). The applied methods included molecular structures similarity study against the cocrystallized ligand (**GWS**) of M^{pro} (PDB ID: 5R84) [42] (Figure 1), molecular fingerprints study against the same ligand, molecular docking, molecular dynamics (MD) simulations and MM-PBSA experiments against M^{pro}.

Unfortunately, the *in vitro* and *in vivo* examinations against COVID-19 are not accessible for our team currently.

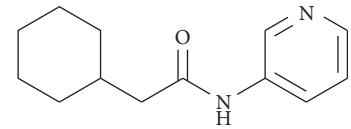

Figure 1: Structure of the cocrystallized ligand (**GWS**) of M^{pro} (PDB ID: 5R84).

However, we employed extensive well-structured *in silico* methods to present a sort of strong potential SARS-CoV-2 inhibitors for every scientist who has these facilities aiming at finding a treatment.

2. Results and Discussion

2.1. Filter Using Fingerprints. The cocrystallized ligand is a compound that strongly binds to a specific protein, forming a crystalized complex [43]. This complex provides crucial insights into the nature of interaction, revealing important structural and chemical characteristics that contribute to the strong binding with that protein [44]. The chemical structural features of the cocrystallized ligand serve as a valuable blueprint for designing inhibitors that can effectively bind to the target protein. By examining the structural features and functional groups of the cocrystallized ligand, we can better understand the key elements responsible for its strong binding [45]. We used this knowledge to select compounds similar to **GWS**, aiming to discover potent inhibitors with a high affinity for the M^{pro} protein (Table 1). This approach is rooted in the principle of a structure-activity relationship (SAR), which suggests that compounds with similar chemical structures are likely to have similar biological effects [46]. The molecular fingerprints analysis represented the absence or existence of the next descriptors in the fragments and atoms of the considered compounds and **GWS**: H-bond acceptors [47], H-bond donors [48], charges [49], hybridization [50], positive ionizable atoms [51], negative ionizable atoms [52], halogens [53], and aromatic groups [54], align with the ALogP [55].

2.2. Molecular Similarity. A fundamental distinction between molecular similarity studies and fingerprint studies lies in the depth of molecular information they capture. Molecular similarity studies embrace a wider array of molecular descriptors and properties, facilitating a comprehensive evaluation of structural and chemical resemblances. These studies encompass considerations such as molecular shape, electrostatic characteristics, and pharmacophoric attributes. In contrast, fingerprint studies focus on specific structural motifs encoded in binary fingerprints, presenting a more condensed representation of molecular structures [56]. In a molecular similarity study, a holistic analysis is conducted, wherein the complete structures of the reference compound and the examination set are characterized and juxtaposed, employing descriptors encompassing steric, topological, electronic, or physicochemical attributes [57]. Molecular structural similarity study also belongs to the approaches of ligand-based *in silico* (computational) type

Table 1: Fingerprint similarity between the tested compounds and **GWS**.

Comp	Similarity	SA	SB	SC
GWS	1.000	176	0	0
18	0.686	168	69	8
58	0.594	174	117	2
68	0.552	137	72	39
74	0.532	158	121	18
92	0.559	176	139	0
114	0.622	217	173	−41
163	0.629	158	75	18
169	0.609	168	100	8
224	0.517	109	35	67
227	0.583	183	138	−7
252	0.613	168	98	8
266	0.595	194	150	−18
276	0.607	167	99	9
279	0.539	213	219	−37
286	0.530	123	56	53
297	0.562	218	212	−42
325	0.536	118	44	58
339	0.533	122	53	54
393	0.554	163	118	13
400	0.583	123	35	53
417	0.571	192	160	−16
419	0.629	158	75	18
438	0.540	218	228	−42
462	0.531	155	116	21
486	0.512	174	164	2
497	0.514	150	116	26
508	0.573	172	124	4
515	0.567	160	106	16
530	0.584	185	141	−9
552	0.587	145	71	31
560	0.558	201	184	−25
614	0.520	130	74	46
643	0.540	154	109	22
671	0.557	230	237	−54
675	0.562	136	66	40
686	0.564	137	67	39
727	0.608	163	92	13
736	0.522	153	117	23
741	0.538	183	164	−7
756	0.524	177	162	−1
768	0.556	140	76	36
772	0.553	210	204	−34
786	0.530	178	160	−2
829	0.542	156	112	20
843	0.572	158	100	18
854	0.646	159	70	17
855	0.590	207	175	−31
863	0.519	285	373	−109
878	0.512	148	113	28
911	0.551	151	98	25
935	0.520	259	322	−83
970	0.558	203	188	−27
987	0.518	142	98	34
1064	0.608	163	92	13
1069	0.573	172	124	4
1108	0.585	226	210	−50
1113	0.582	114	20	62
1168	0.567	136	64	40
1177	0.512	173	162	3

Table 1: Continued.

Comp	Similarity	SA	SB	SC
1178	0.586	190	148	−14
1179	0.564	168	122	8
1186	0.587	138	59	38
1211	0.547	188	168	−12
1253	0.530	151	109	25
1267	0.530	254	303	−78
1284	0.554	206	196	−30
1315	0.548	165	125	11
1320	0.531	155	116	21
1410	0.512	174	164	2
1441	0.523	104	23	72
1443	0.523	104	23	72
1461	0.515	150	115	26
1462	0.535	147	99	29
1463	0.527	97	8	79
1516	0.618	168	96	8
1521	0.523	104	23	72
1551	0.529	208	217	−32
1553	0.514	182	178	−6
1589	0.553	121	43	55
1591	0.549	169	132	7
1604	0.531	170	144	6
1608	0.512	214	242	−38
1622	0.596	121	27	55
1649	0.529	101	15	75
1694	0.547	181	155	−5
1737	0.516	127	70	49
1742	0.595	209	175	−33
1756	0.524	204	213	−28
1805	0.580	170	117	6
1818	0.527	194	192	−18
1822	0.531	241	278	−65
1919	0.564	168	122	8
1955	0.579	169	116	7
1975	0.615	134	42	42
1993	0.547	169	133	7
2023	0.512	127	72	49
2024	0.601	176	117	0
2075	0.606	168	101	8
2091	0.530	96	5	80
2126	0.533	147	100	29
2163	0.682	189	101	−13
2171	0.532	166	136	10
2185	0.550	138	75	38
2205	0.567	174	131	2
2261	0.519	160	132	16
2264	0.584	201	168	−25
2274	0.690	191	101	−15
2296	0.537	110	29	66
2306	0.523	174	157	2
2325	0.602	136	50	40
2333	0.603	185	131	−9
2334	0.632	127	25	49
2351	0.608	158	84	18
2372	0.562	154	98	22
2380	0.614	159	83	17
2384	0.545	126	55	50
2395	0.646	168	84	8
2399	0.530	151	109	25
2403	0.594	168	107	8

Table 1: Continued.

Comp	Similarity	SA	SB	SC
2425	0.532	100	12	76
2437	0.576	179	135	−3
2447	0.573	201	175	−25
2478	0.535	168	138	8
2524	0.597	160	92	16
2525	0.578	170	118	6
2530	0.556	155	103	21
2553	0.550	105	15	71
2603	0.604	116	16	60
2622	0.516	214	239	−38
2630	0.539	138	80	38
2638	0.515	152	119	24
2649	0.636	140	44	36
2657	0.633	143	50	33
2660	0.618	168	96	8
2704	0.561	162	113	14
2761	0.528	239	277	−63
2775	0.603	152	76	24
2788	0.521	126	66	50
2790	0.522	186	180	−10
2825	0.516	145	105	31
2839	0.588	143	67	33
2840	0.606	172	108	4
2865	0.542	156	112	20
2877	0.519	217	242	−41
2901	0.565	140	72	36
2917	0.568	147	83	29
2918	0.540	162	124	14
2939	0.523	229	262	−53
3003	0.607	167	99	9

SA: The number bits in both **GWS** and the target. **SB**: The number of bits in the target but not **GWS**. **SC**: The number of bits in **GWS** but not the target. The bold values indicate that the number is based on the number of compounds.

that considered following descriptors; hydrogen bond donors (HBA) [58], acceptors (HBD) [59] partition coefficient (Alog p) [60], molecular weight (M. W) [61], rotatable bonds [62], rings and aromatic rings [63], and molecular fractional polar surface area (MFPSA) [64]. The computation of the mentioned features using Discovery Studio software led to the revelation of the best 29 analogs (Figure 2, and Table 2).

2.3. Docking Studies

2.3.1. Validation of Molecular Docking. The molecular docking algorithm was initially validated by redocking of the cocrystallized ligand into the active site of the target receptor (SARS-CoV-2 M^{pro} PDB ID: 5R84) with the calculation of root mean square deviation (RMSD) for reliability and reproducibility of the proposed docking algorithm. The redocked ligand showed an RMSD value of 0.56 A indicating a validated docking process (Figure 3).

The binding mode of the cocrystallized ligand (**GWS**) exhibited a binding energy of −6.51 kcal/mol against M^{pro}. The cyclohexyl moiety formed three Pi-Alkyl interactions with His41, Met165, and Met49. Additionally, the amino group in (pyridine-3-yl) acetamide moiety interacted with His163 by one hydrogen bond with a distance of 1.99°A. Moreover, the amide linker interacted with Glu166 and Asn142 by two hydrogen bonds with distances of 2.04 and 2.72°A, respectively (Figure 4).

The binding mode of compound **68** (Ramelteon) exhibited a binding energy of −6.49 kcal/mol against M^{pro}. The tetrahydro-2*H*-indeno[5,4-*b*]furan-8-yl moiety formed three Pi-alkyl interactions with Met49, His41, and Met165. Additionally, the ethyl propionamide moiety formed two hydrogen bonds with Glu166(2.51°A) and Asn142 (2.35°A) (Figure 5).

Compound **224** (Prilocaine) exhibited a binding energy of −6.05 kcal/mol against M^{pro}. The o-tolyl moiety formed three Pi-alkyl and Pi-Pi interactions with Cys145, His163, and Leu141. The amide moiety interacted with Asn142 and Glu166 by two hydrogen bonds with distances of 2.31 and 1.97°A, respectively (Figure 6).

The binding mode of compound **339** (Nefiracetam) exhibited a binding energy of −6.12 kcal/mol against M^{pro}. The 2,6-dimethylphenyl moiety formed three Pi-alkyl interactions with His41 and Met165. The (2-oxopyrrolidin-1-yl) acetamide moiety formed two hydrophobic interactions with His163 and Cys145. Moreover, the central amide moiety interacted with two hydrogen bonds with Asn142 and Glu166 with a distance of 2.42 and 2.01°A, respectively. (Figure 7).

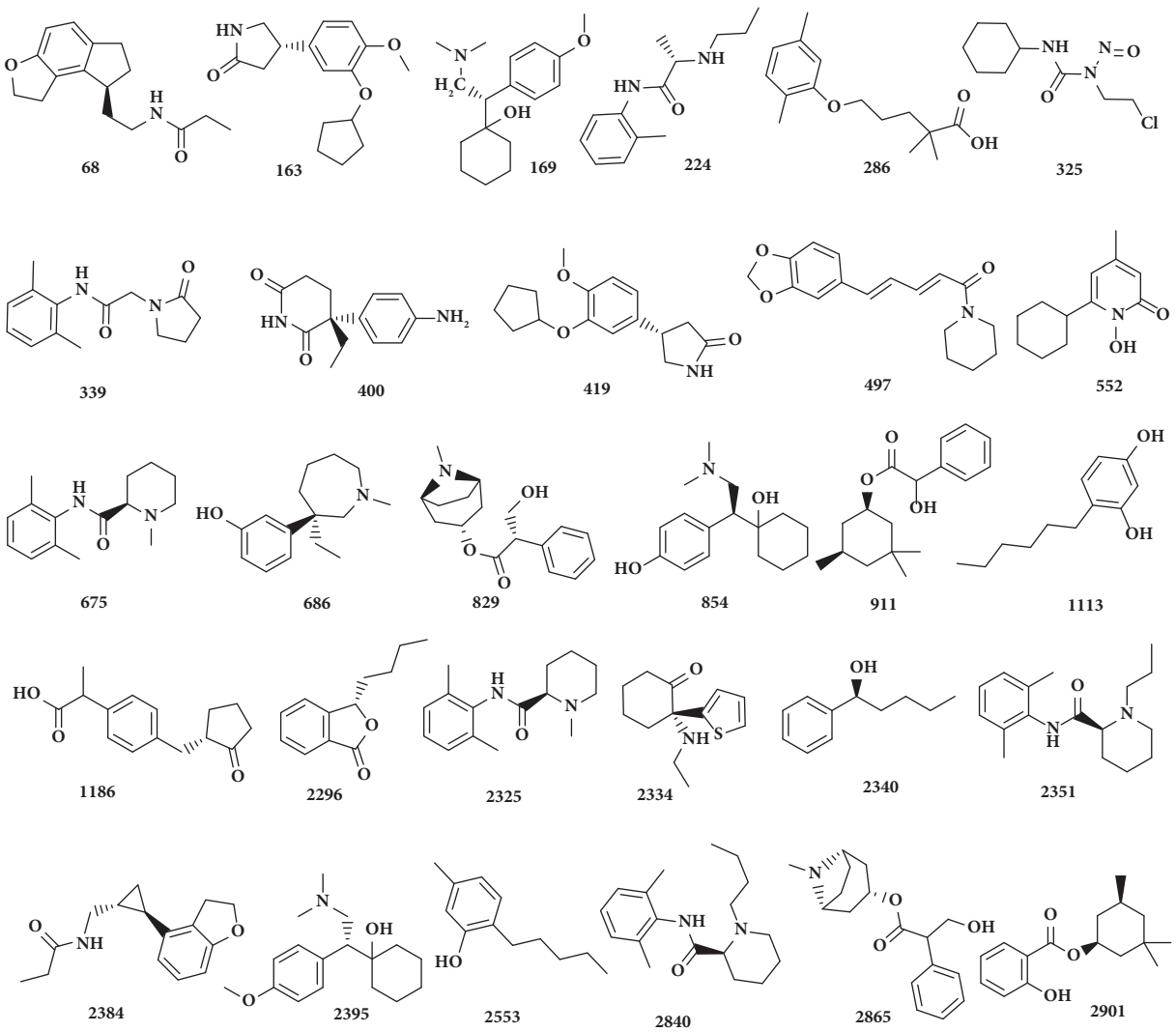

Figure 2: Twenty-nine compounds with good molecular similarity with **GWS**.

Table 2: Molecular descriptors of the examined compounds and **GWS**.

Comp	Alog p	M. Wt	HBA	HBD	Rotatable bonds	Rings	Aromatic rings	MFPSA	Minimum distance
GWS	2.17	218.3	2	1	3	2	1	0.179	0
68	2.83	259.34	2	1	4	3	1	0.143	0.388
163	2.35	275.34	3	1	4	3	1	0.17	0.456
169	3.4	313.86	3	1	5	2	1	0.088	0.733
224	2.26	220.31	2	2	5	1	1	0.157	0.484
286	4.17	250.33	3	1	6	1	1	0.154	0.666
325	2.39	233.7	3	1	4	1	0	0.261	0.732
339	1.44	246.31	2	1	3	2	1	0.182	0.21
400	1.29	232.28	3	2	2	2	1	0.293	0.664
419	2.35	275.34	3	1	4	3	1	0.17	0.456
497	2.86	285.34	3	0	3	3	1	0.132	0.634
552	2.49	207.27	2	1	1	2	0	0.186	0.594
675	3.36	282.81	2	1	2	2	1	0.1	0.532
686	3.91	269.81	2	1	2	2	1	0.074	0.63
829	1.72	289.37	4	1	5	3	1	0.167	0.683
854	2.8	263.38	3	2	4	2	1	0.144	0.526
911	3.64	276.37	3	1	4	2	1	0.149	0.515

Table 2: Continued.

Comp	Alog p	M. Wt	HBA	HBD	Rotatable bonds	Rings	Aromatic rings	MFPSA	Minimum distance
1113	4.11	194.27	2	2	5	1	1	0.181	0.643
1186	2.94	246.3	3	1	4	2	1	0.212	0.364
2296	3.25	190.24	2	0	3	2	1	0.131	0.481
2325	2.98	246.35	2	1	2	2	1	0.114	0.362
2334	2.9	259.8	2	1	3	2	1	0.206	0.281
2340	3.04	164.24	1	1	4	1	1	0.104	0.568
2351	3.85	274.4	2	1	4	2	1	0.102	0.563
2384	2.2	245.32	2	1	4	3	1	0.154	0.311
2395	3.02	277.4	3	1	5	2	1	0.1	0.572
2553	4.39	178.27	1	1	4	1	1	0.093	0.714
2840	4.31	288.43	2	1	5	2	1	0.096	0.703
2865	1.72	289.37	4	1	5	3	1	0.167	0.683
2901	4.01	262.34	3	1	3	2	1	0.158	0.517

The bold values indicate that the number is based on the number of compounds.

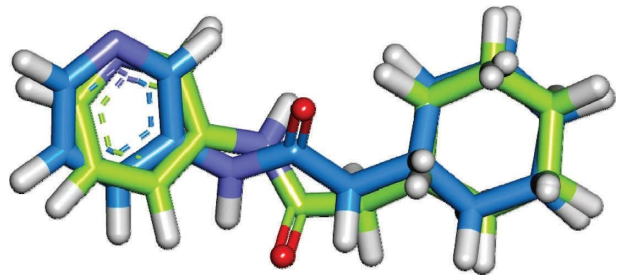

Figure 3: Superimposition of the docked and original poses of the cocrystallized ligand of SARS-CoV-2 $\mathbf{M^{pro}}$ (PDB ID: 5R84).

Compound **911** (Cyclandelate) exhibited a binding energy of −6.89 kcal/mol against M^{pro}. The trimethyl cyclohexyl moiety formed six hydrophobic interactions with His41, Met49, and Met165. Additionally, the 2-hydroxy-2-phenylacetate moiety formed three hydrogen bonds with Glu166, Asn142, and Leu141 with distances of 1.99, 2.45, and 2.55°A, respectively (Figure 8).

Compound **2325** (Mepivacaine) exhibited a binding score of −6.19 kcal/mol. The 2,6-dimethyl phenyl moiety formed three Pi-alkyl and Pi-sulfur interactions with His163 and Cys145. The piperidine moiety formed two Pi-alkyl interactions with His41 and Met49. Moreover, the central amide moiety interacted with two hydrogen bonds with Glu166 and Asn142 with a distance of 2.01 and 2.40°A, respectively (Figure 9).

The binding mode of compound **2351** (Ropivacaine) exhibited an energy binding of −6.38 kcal/mol against M^{pro}. The 2,6-dimethyl phenyl moiety formed three Pi-alkyl and Pi-sulfur interactions with His163 and Cys145. The propylpiperidine moiety formed two Pi-alkyl interactions with His41 and Met49. Moreover, the central amide moiety interacted by two hydrogen bonds with Glu166 and Asn142 with a distance of 2.27 and 2.25°A, respectively (Figure 10).

The binding mode of compound **2384** (Tasimelteon) exhibited an energy binding of −6.45 kcal/mol-1 against M^{pro}. The 2,3-dihydrobenzofuran-4-yl moiety formed four Pi-alkyl and Pi-Pi interactions with Met49, Met165, and His41. Additionally, it formed one hydrogen bond with Glu166 at a distance of 2.44°A. The (cyclopropyl methyl) propionamide moiety interacted with Asn142 through one hydrogen bond with a distance of 2.63°A. Moreover, it was incorporated in four Pi-alkyl interactions with His163, His172, His41, and Cys145 (Figure 11).

Interestingly, the binding mode of compound **2840** (Levobupivacaine) was very similar to that of the cocrystallized ligand (**GWS**) exhibiting a binding energy of −6.65 kcal/mol, slightly bitter that **GWS** (−6.51 kcal/mol) against the M^{pro}. In detail, The 2,6-dimethylphenyl moiety of compound **2840**, in a similar way to the cyclohexyl moiety of **GWS** formed hydrophobic interactions with the same three amino acids; Met49, His41, and Met165. Additionally, the butylpiperidine moiety of compound **2840** interacted with Asn142 by a hydrogen bond with a distance of 2.36°A. The amide linker of **GWS** interacted with the same amino acid through a hydrogen bond with distances of 2.72°A. Furthermore, the butylpiperidine moiety of compound **2840** formed one hydrophobic interaction with His163 similar to the amino group in (pyridine-3-yl) acetamide moiety of **GWS**. Finally, the amide linker of compound **2840** formed two hydrogen bonds with Gln189, and Glu166 in a distance of 2.24, and 2.64°A, respectively. This interaction was similar to that of the amide linker of **GWS** with Glu166 a hydrogen bond with a distance of 2.04°A. In summary, compound **2840** (Levobupivacaine) exhibited interactions with all the amino acids that the cocrystallized ligand (**GWS**) interacted with. Additionally, there was an extra interaction observed with Gln189 (Figure 12, and Table 3).

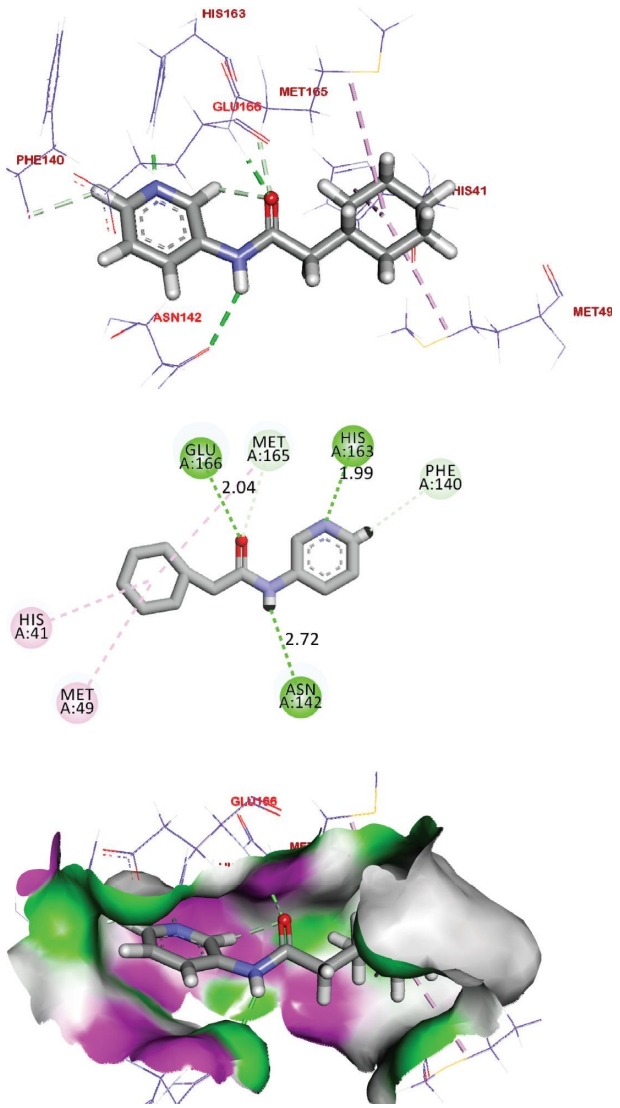

Figure 4: Binding mode and mapping surface of **GWS** in the active site of M^{pro}.

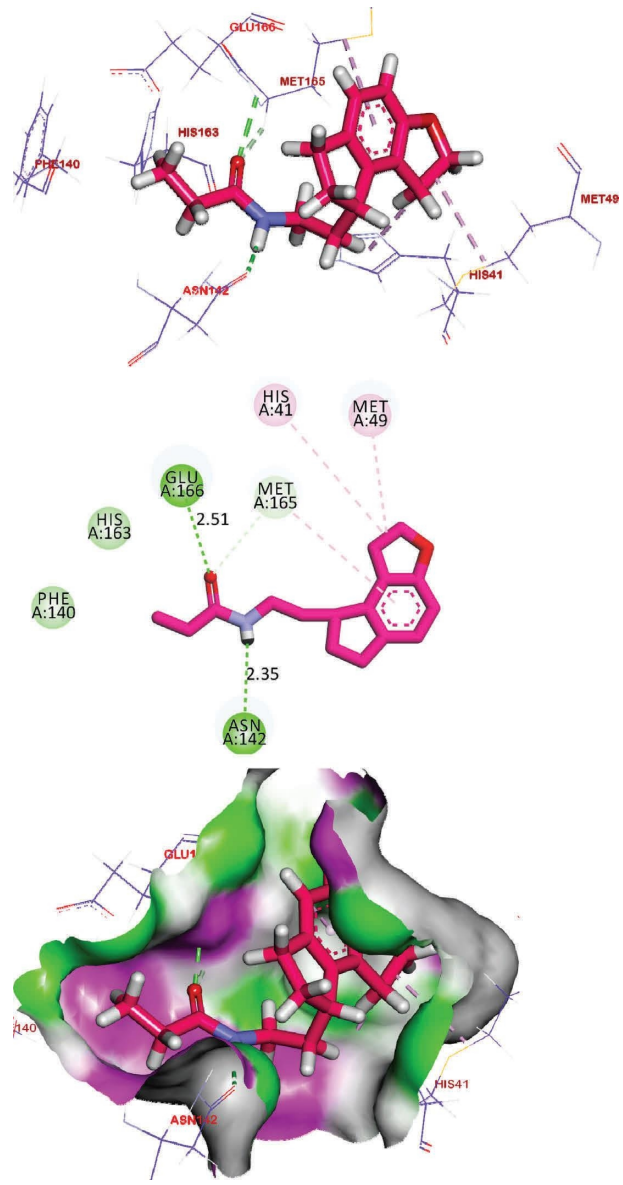

Figure 5: Binding mode and mapping surface of compound **68** in the active site of M^{pro}.

2.4. Pharmacophore Study. The pharmacophore recognizes the key features in a ligand to interact with a protein target resulting in elicitation or blockage of a certain biological activity. The 3D pharmacophore model determines the essential chemical feature of a metabolite to be active against a specific protein. Additionally, it specifies the 3D geometry of these essential features [65]. The generated 3D model is an important key that can be used to predict definite bioactivity based on the presence or absence of these features [66, 67]. The presented study concerned the optimization of the key pharmacophoric interaction features of the cocrystallized ligand (**GWS**) of the main protease (PDB ID: 5R84) and the consequent examination of the presence of these features in the tested FDA-approved drug to pick the most promising candidates.

2.4.1. Generation of a 3D-Pharmacophore Model. The generated 3D pharmacophore model consisted of three features: one H-bond donor and two hydrophobic centers (Figure 13(a)). The generated model was used as a 3D search query to evaluate the tested drugs as possible SARS-CoV-2 main protease inhibitors. The fitting of the cocrystallized ligand against the generated pharmacophore model was illustrated in Figure 13(b).

2.4.2. The Test Set Activity Prediction. The test set of thirty FDA-approved drugs was mapped to the generated 3D pharmacophore model. As a result, the FDA-approved drugs that verified the essential pharmacophoric features and the fit value were selected as promising candidates.

The results privileged nineteen drugs that have the main essential features of SARS-CoV-2 main protease inhibitors. Surprisingly, the drugs that showed good binding mode against SARS-CoV-2 main protease showed high fit and high relative fit values. In detail, compounds **68** (Fit value = 2.86,

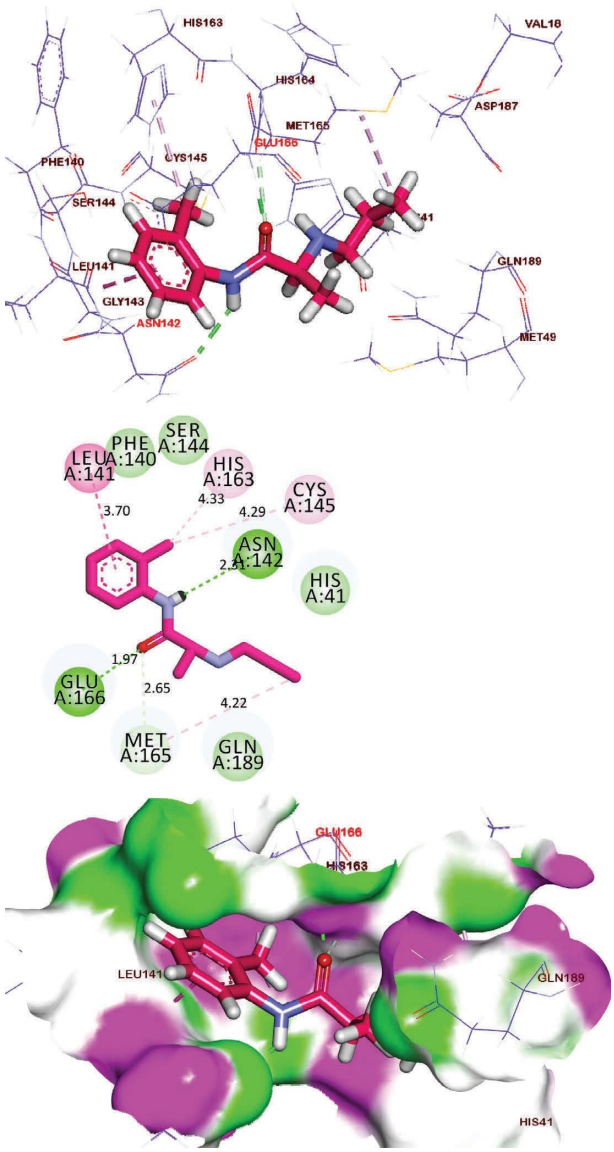

Figure 6: Binding mode and mapping surface of compound **224** in the active site of M^{pro}.

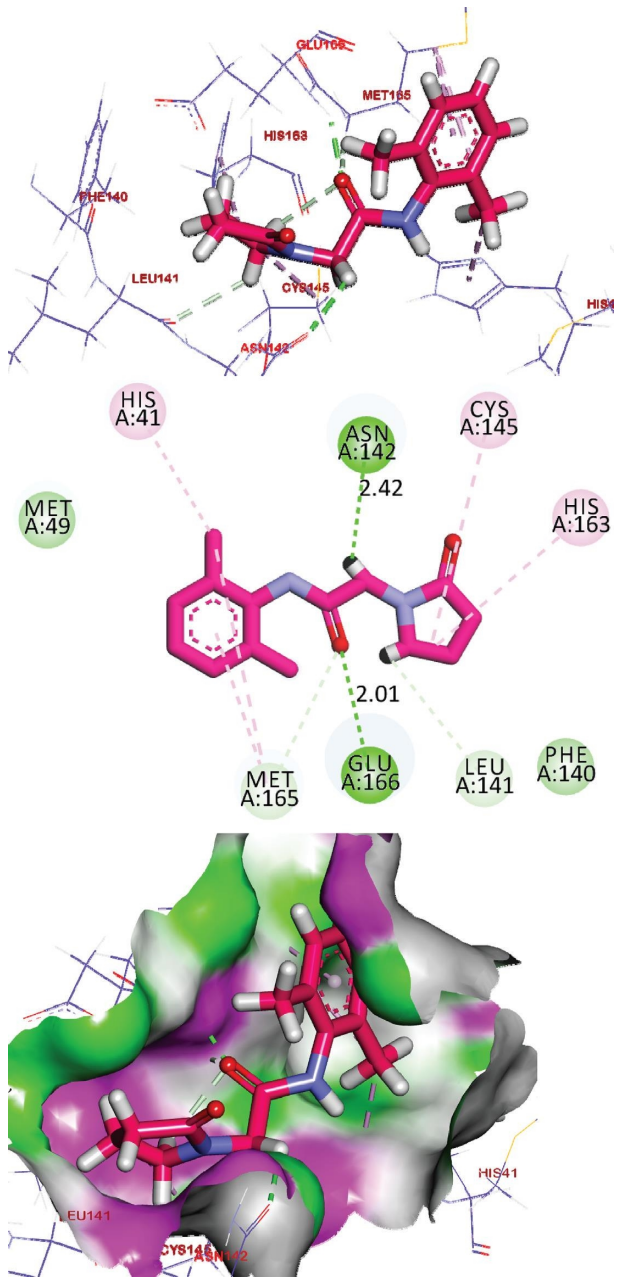

Figure 7: Binding mode and mapping surface of compound **339** in the active site of M^{pro}.

Relative Fit = 74.48%), **224** (Fit value = 2.75, Relative Fit = 96.15%), **339** (Fit value = 2.56, Relative Fit = 89.51), **911** (Fit value = 2.81, Relative Fit = 98.25%), **2325** (Fit value = 2.73, Relative Fit = 95.45%), **2351** (Fit value = 2.75, Relative Fit = 96.15%), **2384** (Fit value = 2.38, Relative Fit = 83.22%), and **2840** (Fit value = 2.78, Relative Fit = 97.20%) showed high fit value comparing to the cocrystallized ligand (Fit value = 2.86, Relative Fit = 100%) (Table 4).

Figure 14 shows the mapping of the most promising drugs that showed good fitting value against the generated 3D-pharmacophore and well as good binding mode against SARS-CoV-2 main protease.

In summation, eight compounds were appointed as potential M^{pro} inhibitors (ramelteon (**68**), prilocaine (**224**), nefiracetam (**339**), cyclandelate (**911**), mepivacaine (**2325**), ropivacaine (**2351**), tasimelteon (**2384**), and levobupivacaine (**2840**)). levobupivacaine (**2840**) demonstrated identical 3D pharmacophore features to the cocrystallized ligand (**GWS**), encompassing HBD-1, hydrophobic-2, and aromatic ring-3. Notably, levobupivacaine (**2840**) displayed the highest fit value at 2.78, accompanied by the highest relative Fit of 97.20%. Ramelteon, the melatonin agonist, is used to treat insomnia [68]. Interestingly, Ramelteon demonstrated significant *in silico* anti-SARS-CoV-2 activities through binding and inhibition of SARS-CoV-2 RBD and ACE 2 [69]. A drug repositioning study identified prilocaine as a potential candidate against COVID-19 [70]. Stimulatingly, cyclandelate showed *in vitro* inhibitory effect against 1 ribosomal frameshifting of SARS-CoV-2 at a concentration of 2 μM

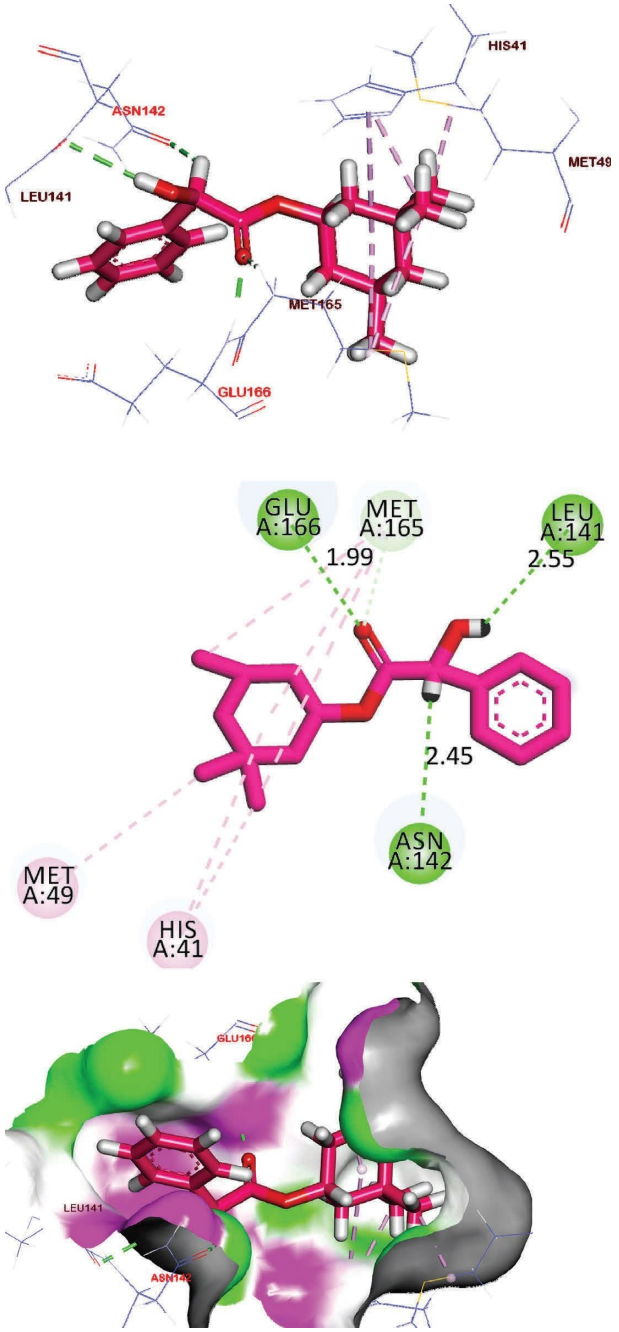

Figure 8: Binding mode and mapping surface of compound **911** in the active site of M^{pro}.

[71]. Additionally, mepivacaine, the local anesthetic, demonstrated an *in vitro* inhibitory effect against Herpes simplex 1 before [72]. Further, tasimelteon displayed significant *in silico* binding with the COVID-19 PLpro [73]. Also, a molecular modeling study suggested the anti-COVID-19 potential of the local anesthetic, levobupivacaine [74]. On the other side, this is the first time to referee an antiviral potentiality for both nefiracetam and ropivacaine. Because several selected compounds are local anesthetics, further studies regarding the route of administration and systemic safety of these drugs are essential.

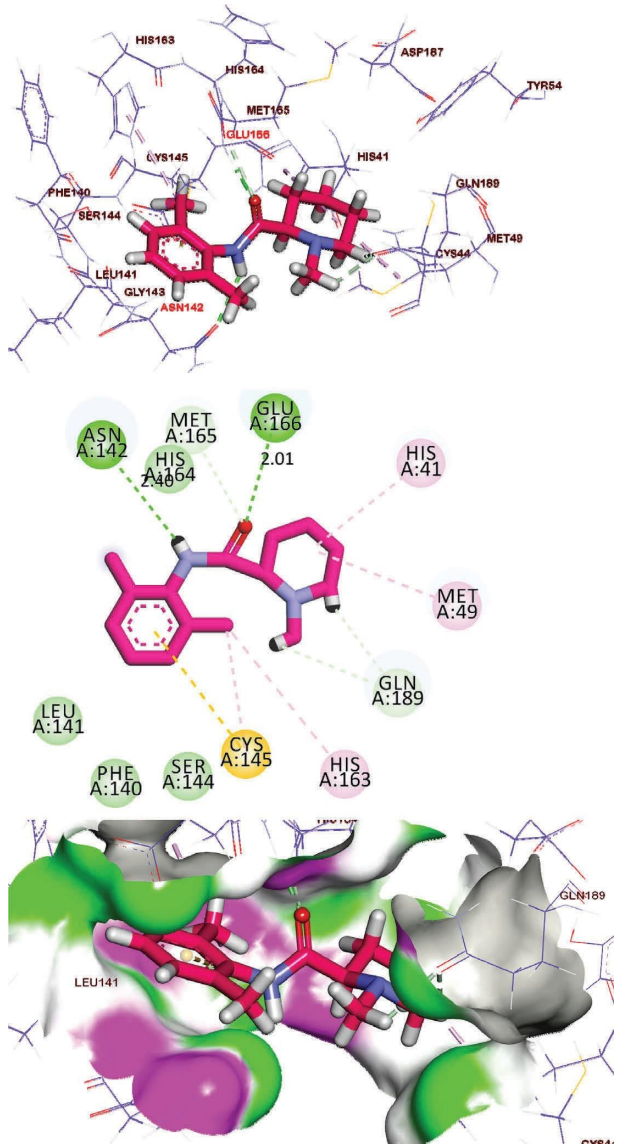

Figure 9: Binding mode and mapping surface of compound **2325** in the active site of M^{pro}.

2.5. Molecular Dynamic Simulations. Molecular dynamics (MD) simulations can be used to examine almost all sorts of big molecules (proteins, nucleic acids, and carbohydrates) of medicinal significance. The MD experiments can supply not only galore energetic records on the considered macromolecules but also a considerable of dynamical structural specifics about the interactions that happen between the ligand and the targeted protein. The acquired information is very beneficial to understand several parameters regarding the protein-ligand interaction [75]. Being an effective guide, MD simulations experiments have been applied widely and successfully in the process of modern drug discovery and discovery [76].

Levobupivacaine (**2840**) demonstrated excellent fitting value against the generated 3D-pharmacophore as well as an ideal binding mode against M^{pro}. Consequently, it was selected for further molecular dynamic simulations.

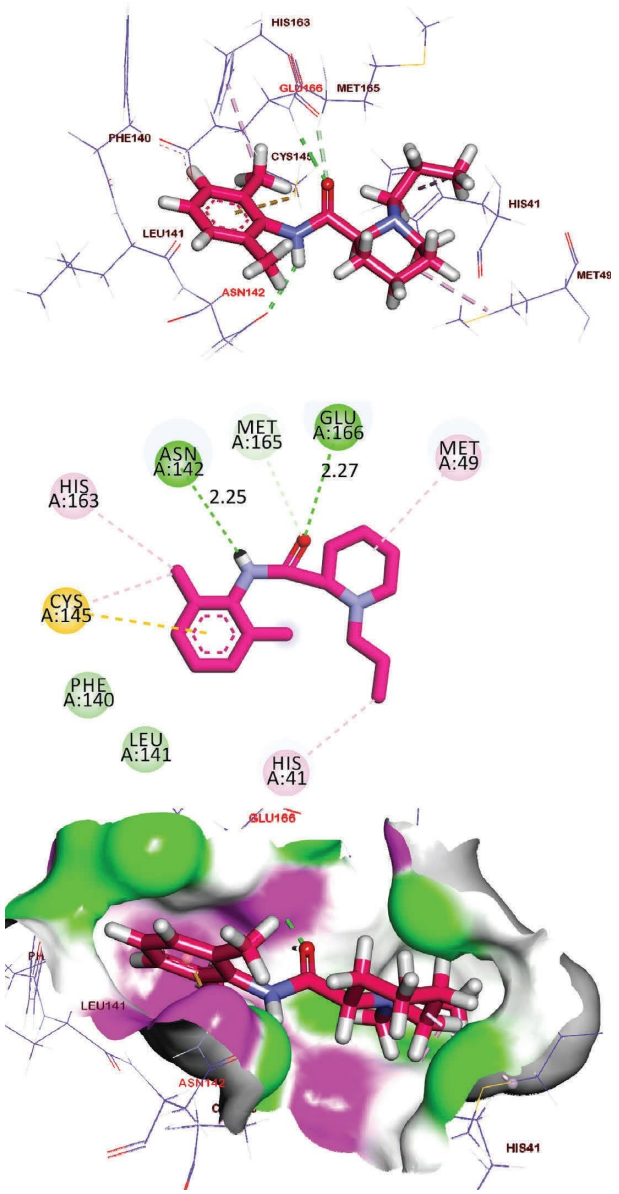

Figure 10: Binding mode and mapping surface of compound **2351** in the active site of M^{pro}.

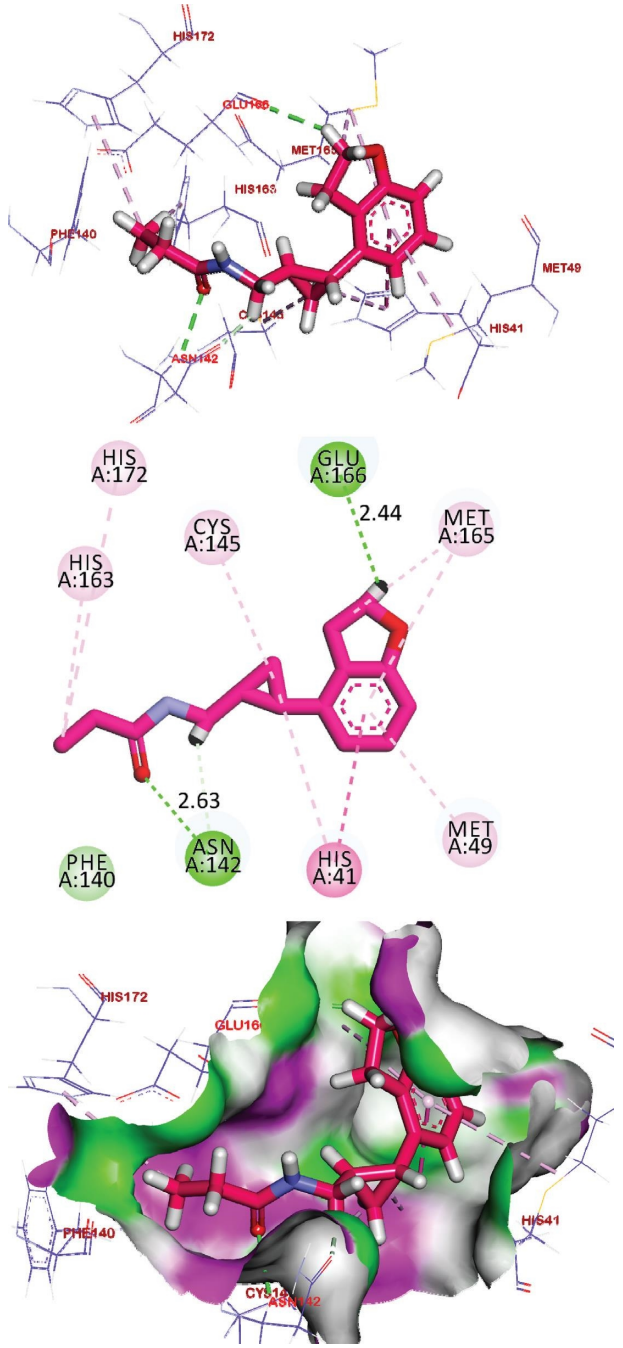

Figure 11: Binding mode and mapping surface of compound **2384** in the active site of M^{pro}.

The dynamic structural changes of the backbone of the levobupivacaine—M^{pro} complex were calculated on an atomic resolution by RMSD to investigate the stability of the explored complex after binding. Stimulatingly, levobupivacaine—M^{pro} complex displayed a low value of root mean square deviation (RMSD) exhibiting no major fluctuations (Figure 15(a)). This outcome indicates the stability of the reviewed complex. The flexibility of the levobupivacaine—M^{pro} complex was diagnosed in terms of root mean square fluctuation (RMSF) to expose the fluctuated regions of M^{pro} during the simulation. It was confirmed that the binding of levobupivacaine does not change the flexibility of M^{pro} significantly (Figure 15(b)). To study the compactness of the levobupivacaine—M^{pro} complex, the radius of gyration (Rg) of M^{pro} was computed. The Rg of the M^{pro} was more constant at the end of the experiment than at the starting period (Figure 15(c)). Interaction between levobupivacaine—M^{pro} complex and the surrounding solvents was estimated by solvent accessible surface area (SASA) over a period of 100 ns. Fortunately, the levobupivacaine—M^{pro} complex featured a noticeable decrease in the surface area (lower SASA value) than the starting time (Figure 15(d)). Hydrogen bonding through the Levobupivacaine—M^{pro} complex was estimated over 100 ns. Favorably, the highest number of the M^{pro} conformations formed up to two hydrogen bonds with the Levobupivacaine over the examined 100 ns (Figure 15(e)).

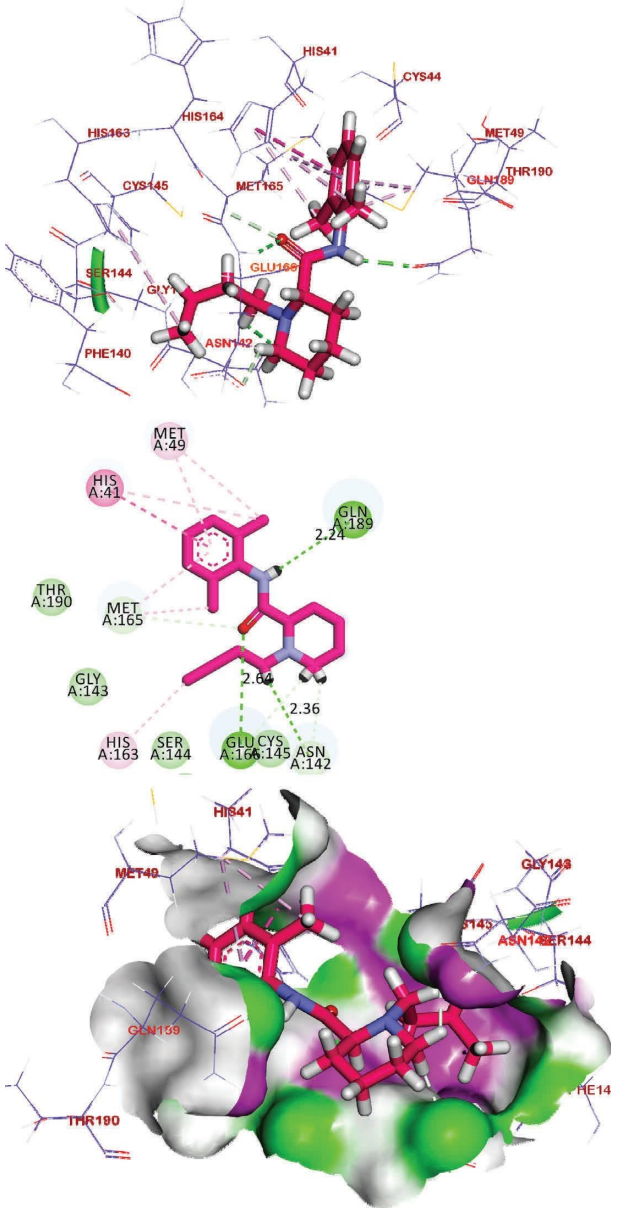

Figure 12: Binding mode and mapping surface of compound **2840** in the active site of M^{pro}.

2.6. MM-PBSA. The molecular mechanics Poisson–Boltzmann surface area (MM-PBSA) is a computational technique employed in molecular modeling and computational chemistry to estimate the binding free energy between a ligand and a protein. This method combines molecular mechanics (MM) computations, which elucidate interactions within the complex, with Poisson–Boltzmann (PB) computations, which factor in the electrostatic interactions between the solute and its surrounding solvent environment [77].

In the MM-PBSA approach, the binding free energy (ΔG_bind) is approximated by evaluating the energetic components associated with the complex, the ligand, and the receptor in both bound and unbound states. These components encompass contributions from van der Waals interactions, electrostatic interactions, and alterations in solvation-free energy [78]. MM-PBSA is especially valuable for investigating interactions between proteins and ligands, offering insights into the thermodynamics of binding and aiding in the design of potential drug compounds. It is important to acknowledge, however, that while MM-PBSA provides valuable estimates, it relies on several assumptions and may not capture the complete intricacies of binding processes in all systems [79]. We calculated the binding free energy of the last 20 ns of MD production run of the levobupivacaine—M^{pro} complex with an interval of 100 ps from MD trajectories using the MM/PBSA method. As shown in Figure 16(a), Levobupivacaine displayed an excellent binding free energy of −235 kJ/mol with the M^{pro}. Furthermore, the participation of each amino acid residue of the M^{pro} regarding the binding free energy after the binding with levobupivacaine was computed. The total binding free energy of the levobupivacaine—M^{pro} complex was decomposed into per amino acid residue contribution energy. The output of this study helps to identify the essential amino acid residues in the binding of the levobupivacaine—M^{pro} complex. It was found that GLU-47, ASP-48, GLU-55, ASP-56, GLU-166 and ASP-187 residues of the M^{pro} shared higher than −15 kJ/mol binding energy (Figure 16(b)). It is noteworthy to mention that GLU-166, an essential amino acid, was identified in the interactions of both levobupivacaine and the cocrystallized ligand (**GWS**).

3. Method

3.1. Molecular Similarity Detection. Compound similarity was assessed in Discovery Studio 4.0 using the CHARMM force field and ligand preparation protocol. Compounds were compared to **GWS** with a 5% output adjustment. Default molecular properties were used, including rotatable bonds, rings, aromatic rings, HBA, HBD, ALog p, M. Wt, and MFPSA. The study was operated by Discovery Studio 4.0 software as represented before [80] (additional details in Supplementary data).

3.2. Fingerprint Studies. Compound fingerprints were evaluated against **GWS** using Discovery Studio 4.0. CHARMM force field was initially applied, and compounds were prepared using the ligand protocol. They were then compared to **GWS**. Default molecular properties were used, including various atom parameters. This encompassed charge, hybridization, H-bond features, ionizability, halogenation, aromaticity, or none of the above. Additionally, ALogP category of atoms was considered. The study was operated by Discovery Studio 4.0 software as represented before [81] (additional details in Supplementary data).

3.3. Docking Studies. The crystal structure of M^{pro} was obtained from Protein Data Bank. The docking investigation was accomplished using MOE2014. The study was operated by MOE and Discovery Studio 4.0 software [82] as represented before (additional details in Supplementary data).

Table 3: Docking binding energy (kcal/mol) of the tested compounds against M^{pro} (PDB ID: 5R84).

Serial	Compounds	Name	RMSD value (Å)	Docking score (kcal/mol)	No. of H-bonds	No. of hydrophobic bonds
1	**GWS**		0.56	−6.51	3	3
2	**68**	Ramelteon	1.45	−6.49	2	3
3	**163**	Rolipram	1.68	−5.64	1	2
4	**169**	Venlafaxine hydrochloride	1.20	−5.98	1	3
5	**224**	Prilocaine	1.19	−6.05	2	4
6	**286**	Gemfibrozil	1.29	−6.23	3	6
7	**325**	Lomustine	1.11	−5.98	2	2
8	**339**	Nefiracetam	1.23	−6.12	2	5
9	**400**	Aminoglutethimide	1.13	−5.73	0	2
10	**419**	S-(+)-Rolipram	0.91	−6.35	1	3
11	**497**	Piperine	0.89	−6.23	1	3
12	**552**	Ciclopirox	1.56	−5.65	2	0
13	**675**	Mepivacaine hydrochloride	0.78	−6.05	2	3
14	**686**	Meptazinol hydrochloride	1.11	−5.78	0	3
15	**829**	Hyoscyamine	1.40	−6.15	1	3
16	**854**	Desvenlafaxine	1.23	−5.64	2	2
17	**911**	Cyclandelate	1.38	−6.89	3	6
18	**1113**	Hexylresorcinol	0.67	−5.80	1	3
19	**1186**	Loxoprofen	0.88	−6.40	2	1
20	**2296**	3-n-Butylphathlide	0.85	−5.64	0	3
21	**2325**	Mepivacaine	0.85	−6.19	2	5
22	**2334**	Tiletamine Hydrochloride	1.09	−5.80	0	3
23	**2340**	Fenipentol	0.95	−5.78	1	0
24	**2351**	Ropivacaine	1.36	−6.38	2	5
25	**2384**	Tasimelteon	0.89	−6.45	2	8
26	**2395**	Venlafaxine	1.41	−6.44	2	3
27	**2553**	Amylmetacresol	1.25	−5.66	1	2
28	**2840**	Levobupivacaine	0.75	−6.65	3	7
29	**2865**	Atropine	1.36	−6.01	1	3
30	**2901**	Homosalate	0.89	−5.36	0	6

The bold values indicate that the number is based on the number of compounds.

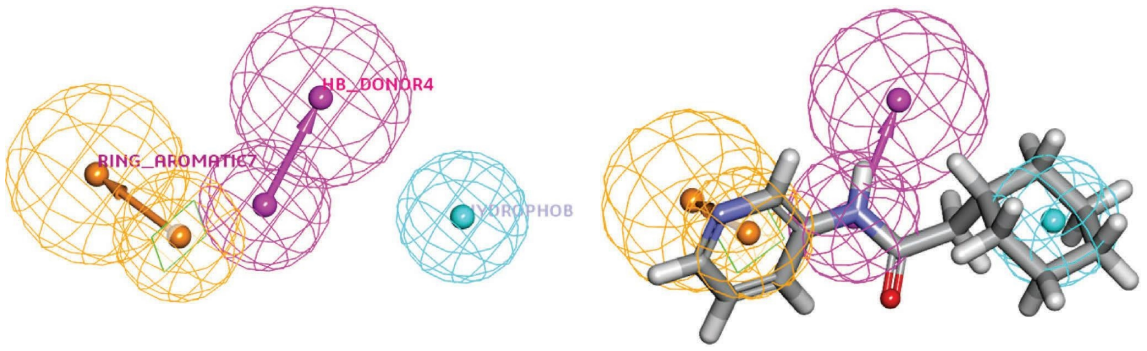

(a) (b)

Figure 13: (a) The generated 3D-pharmacophore geometry with three features; one H-bond donor (pink color) and two hydrophobic centers (blue). (b) Mapping of the cocrystallized ligand on the generated pharmacophore (Fit value = 2.86).

3.4. Pharmacokinetic Profiling. LigandScout software was used to generate a 3D pharmacophore model based on **GWS** binding against M^{pro}. The Espresso algorithm was employed. The best model, which includes features such as hydrogen bond acceptors, donors, aromatic rings, and hydrophobic elements while excluding a volume sphere, was selected from the ten generated models. Model validation was performed using ROC Curve and AUC analysis with default parameters in LigandScout. Discovery Studio 4.0 was used (see method part in Supplementary data).

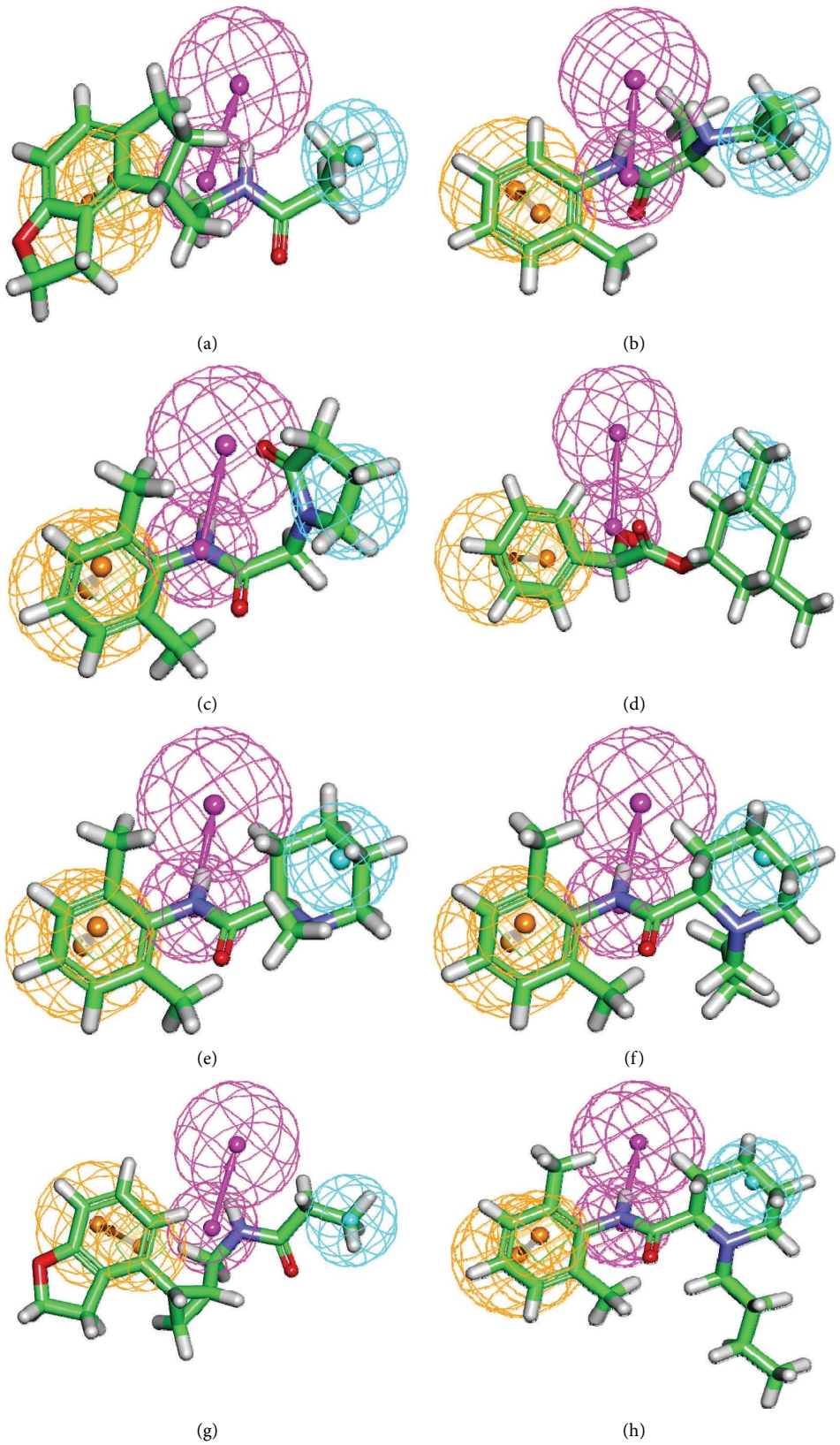

Figure 14: Mapping of the tested metabolites on the generated pharmacophore (a) compounds **68** (Fit value = 2.86, Relative Fit = 74.48%), (b) **224** (Fit value = 2.75, Relative Fit = 96.15%), (c) **339** (Fit value = 2.56, Relative Fit = 89.51), (d) **911** (Fit value = 2.81, Relative Fit = 98.25%), (e) **2325** (Fit value = 2.73, Relative Fit = 95.45%), (f) **2351** (Fit value = 2.75, Relative Fit = 96.15%), (g) **2384** (Fit value = 2.38, Relative Fit = 83.22%), and (h) **2840** (Fit value = 2.78, Relative Fit = 97.20%).

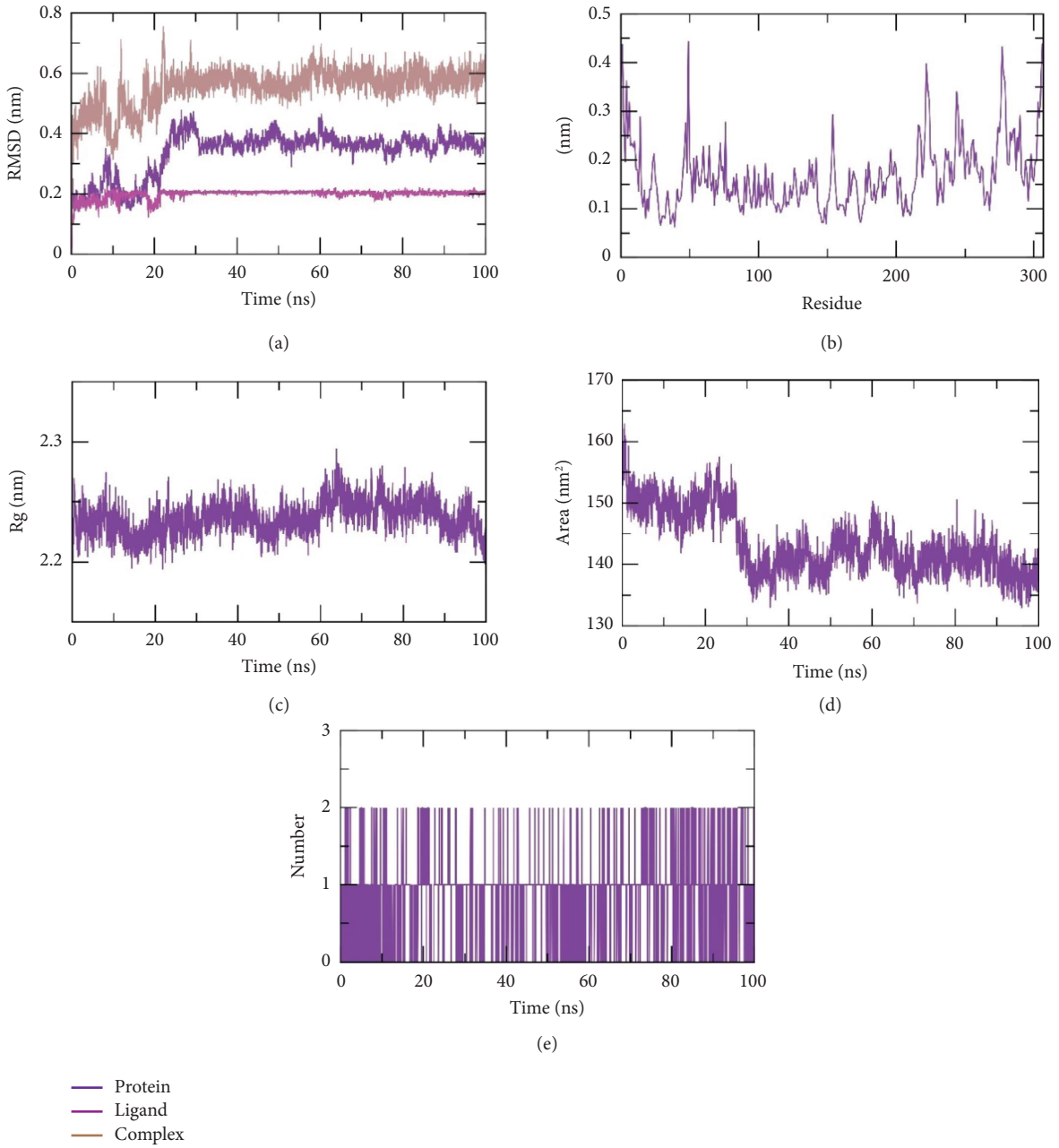

Figure 15: M D simulations outcomes; (a) RMSD values, (b) RMSF, (c) R_g, (d) SASA, and (e) H-bonding between levobupivacaine—M^{pro} complex over 100 ns of the MD run.

Table 4: Fit value and relative fit of the tested metabolites and (**GWS**).

	Comp	Mapped features	Fit value[a]	Relative Fit[b] (%)
1	Cocrystallized ligand	HBD-1, Hydrophobic-2, Aromatic ring-3	2.86	100.00
2	**68**	HBD-1, Hydrophobic-2, Aromatic ring-3	2.13	74.48
3	**169**	HBD-1, Hydrophobic-2, Aromatic ring-3	1.66	58.04
4	**224**	HBD-1, Hydrophobic-2, Aromatic ring-3	2.75	96.15
5	**339**	HBD-1, Hydrophobic-2, Aromatic ring-3	2.56	89.51
6	**675**	HBD-1, Hydrophobic-2, Aromatic ring-3	2.73	95.45
7	**829**	HBD-1, Hydrophobic-2, Aromatic ring-3	2.30	80.42
8	**854**	HBD-1, Hydrophobic-2, Aromatic ring-3	1.76	61.54
9	**911**	HBD-1, Hydrophobic-2, Aromatic ring-3	2.81	98.25
10	**1113**	HBD-1, Hydrophobic-2, Aromatic ring-3	2.66	93.01

Table 4: Continued.

	Comp	Mapped features	Fit value[a]	Relative Fit[b] (%)
11	**2325**	HBD-1, Hydrophobic-2, Aromatic ring-3	2.73	95.45
12	**2334**	HBD-1, Hydrophobic-2, Aromatic ring-3	1.61	56.29
13	**2340**	HBD-1, Hydrophobic-2, Aromatic ring-3	2.76	96.50
14	**2351**	HBD-1, Hydrophobic-2, Aromatic ring-3	2.75	96.15
15	**2384**	HBD-1, Hydrophobic-2, Aromatic ring-3	2.38	83.22
16	**2395**	HBD-1, Hydrophobic-2, Aromatic ring-3	1.62	56.64
17	**2553**	HBD-1, Hydrophobic-2, Aromatic ring-3	2.49	87.06
18	**2840**	HBD-1, Hydrophobic-2, Aromatic ring-3	2.78	97.20
19	**2865**	HBD-1, Hydrophobic-2, Aromatic ring-3	2.30	80.42
20	**2901**	HBD-1, Hydrophobic-2, Aromatic ring-3	2.58	90.21

[b]Relative fit = (fit value of a metabolite/fit value of (**GWS**)) X 100. The bold values indicate that the number is based on the number of compounds.

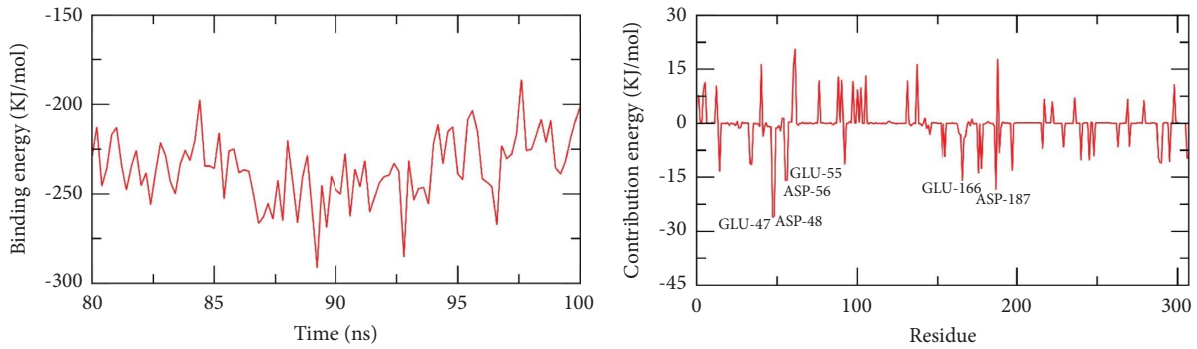

Figure 16: MM-PBSA outcomes of levobupivacaine—M^{pro} complex.

3.5. Molecular Dynamics Simulation. The system was prepared using the web-based CHARMM-GUI [83–85] interface utilizing CHARMM36 force field [86] and NAMD 2.13 [87] package. The TIP3P explicit solvation model was used (additional details in Supplementary data).

3.6. MM-PBSA Studies. The g_mmpbsa package of GROMACS was utilized to calculate the MM/PBSA (additional details in Supplementary data).

4. Conclusion

In conclusion, our study identified eight promising compounds (ramelteon, prilocaine, nefiracetam, cyclandelate, mepivacaine, ropivacaine, tasimelteon, and levobupivacaine) as potential inhibitors against SARS-CoV-2 main protease (M^{pro}). These compounds were selected from a pool of 3009 FDA and clinically approved compounds using a rigorous *in silico* approach. Further analysis through molecular fingerprints, structure similarity, and molecular docking studies confirmed their potential. Levobupivacaine exhibited the highest docking and pharmacophore scores, leading to extensive molecular dynamics simulations. The results demonstrated stable binding and optimal dynamics of the M^{pro}-Levobupivacaine complex over 100 ns. MM-PBSA studies reaffirmed the strong interaction with a free energy value of −235 kJ/mol. These findings provide a promising foundation for further *in vitro* and *in vivo* research on these compounds in the fight against COVID-19.

Data Availability

The data used to support the findings of this study are included within the article.

Conflicts of Interest

The authors declare that they have no conflicts of interest.

Acknowledgments

The authors acknowledge financial support from the Researchers Supporting Project number (RSP-2024/103), King Saud University, Riyadh, Saudi Arabia.

Supplementary Materials

Detailed methodologies covering fingerprints, molecular similarity, molecular docking, pharmacophore, MD simulations, and MM-PBSA studies. (*Supplementary Materials*)

References

[1] Who, "WHO coronavirus (COVID-19) dashboard," 2022, https://covid19.who.int/.

[2] Q. Wang, L. Yang, H. Jin, and L. Lin, "Vaccination against COVID-19: a systematic review and meta-analysis of acceptability and its predictors," *Preventive Medicine*, vol. 150, Article ID 106694, 2021.

[3] H. S. Chan, H. Shan, T. Dahoun, H. Vogel, and S. Yuan, "Advancing drug discovery via artificial intelligence," *Trends in Pharmacological Sciences*, vol. 40, no. 10, 2019.

[4] A. Talevi and C. L. Bellera, "Challenges and opportunities with drug repurposing: finding strategies to find alternative uses of therapeutics," *Expert Opinion on Drug Discovery*, vol. 15, no. 4, pp. 397–401, 2020.

[5] V. Parvathaneni, N. S. Kulkarni, A. Muth, and V. Gupta, "Drug repurposing: a promising tool to accelerate the drug discovery process," *Drug Discovery Today*, vol. 24, no. 10, pp. 2076–2085, 2019.

[6] S. Pushpakom, F. Iorio, P. A. Eyers et al., "Drug repurposing: progress, challenges and recommendations," *Nature Reviews Drug Discovery*, vol. 18, no. 1, pp. 41–58, 2019.

[7] P. Nowak-Sliwinska, L. Scapozza, and A. Ruiz i Altaba, "Drug repurposing in oncology compounds, pathways, phenotypes and computational approaches for colorectal cancer," *Biochimica et Biophysica Acta (BBA) Reviews on Cancer*, vol. 1871, no. 2, pp. 434–454, 2019.

[8] T. U. Singh, S. Parida, M. C. Lingaraju, M. Kesavan, D. Kumar, and R. K. Singh, "Drug repurposing approach to fight COVID-19," *Pharmacological Reports*, vol. 72, no. 6, pp. 1479–1508, 2020.

[9] J. Hong and M. Bang, "Anti-inflammatory strategies for schizophrenia: a review of evidence for therapeutic applications and drug repurposing," *Clinical Psychopharmacology and Neuroscience*, vol. 18, no. 1, pp. 10–24, 2020.

[10] A. K. Konreddy, G. U. Rani, K. Lee, and Y. Choi, "Recent drug-repurposing-driven advances in the discovery of novel antibiotics," *Current Medicinal Chemistry*, vol. 26, no. 28, pp. 5363–5388, 2019.

[11] D.-A. Shirley, I. Sharma, C. A. Warren, and S. Moonah, "Drug repurposing of the alcohol abuse medication disulfiram as an anti-parasitic agent," *Frontiers in Cellular and Infection Microbiology*, vol. 11, Article ID 633194, 2021.

[12] J. Trivedi, M. Mohan, and S. N. Byrareddy, "Drug repurposing approaches to combating viral infections," *Journal of Clinical Medicine*, vol. 9, no. 11, p. 3777, 2020.

[13] S. Ranjan, R. Devarapalli, S. Kundu et al., "Isomorphism: `molecular similarity to crystal structure similarity' in multicomponent forms of analgesic drugs tolfenamic and mefenamic acid," *IUCrJ*, vol. 7, no. 2, pp. 173–183, 2020.

[14] A. T. Baidya, K. Ghosh, S. A. Amin et al., "In silico modelling, identification of crucial molecular fingerprints, and prediction of new possible substrates of human organic cationic transporters 1 and 2," *New Journal of Chemistry*, vol. 44, no. 10, pp. 4129–4143, 2020.

[15] Y. Shi, "Support vector regression-based QSAR models for prediction of antioxidant activity of phenolic compounds," *Scientific Reports*, vol. 11, no. 1, pp. 8806–8809, 2021.

[16] M. O. Idris, A. A. Yekeen, O. S. Alakanse, and O. A. Durojaye, "Computer-aided screening for potential TMPRSS2 inhibitors: a combination of pharmacophore modeling, molecular docking and molecular dynamics simulation approaches," *Journal of Biomolecular Structure and Dynamics*, vol. 39, no. 15, pp. 5638–5656, 2021.

[17] Y. Lu and M. Li, "A new computer model for evaluating the selective binding affinity of phenylalkylamines to T-Type Ca2+ channels," *Pharmaceuticals*, vol. 14, no. 2, p. 141, 2021.

[18] A. Zhanzhaxina, Y. Suleimen, A. M. Metwaly et al., "In vitro and in silico cytotoxic and antibacterial activities of a diterpene from cousinia alata schrenk," *Journal of Chemistry*, vol. 2021, Article ID 5542455, 11 pages, 2021.

[19] R. Jalmakhanbetova, E. B. Elkaeed, I. H. Eissa, A. M. Metwaly, and Y. M. Suleimen, "Synthesis and molecular docking of some grossgemin amino derivatives as tubulin inhibitors targeting colchicine binding site," *Journal of Chemistry*, vol. 2021, Article ID 5586515, 10 pages, 2021.

[20] A. M. Metwaly, V. O. Imieje, A. A. Zaki et al., "Antileishmanial derivatives of humulene from Asteriscus hierochunticus with in silico tubulin inhibition potential," *Records of Natural Products*, vol. 16, no. 2, pp. 150–171, 2021.

[21] M. O. Rafi, K. Al-Khafaji, T. T. Tok, and M. S. Rahman, "Computer-based identification of potential compounds from Salviae miltiorrhizae against Neirisaral adhesion A regulatory protein," *Journal of Biomolecular Structure and Dynamics*, vol. 40, no. 10, pp. 4301–4313, 2020.

[22] D. R. Parmar, J. Y. Soni, R. Guduru et al., "Discovery of new anticancer thiourea-azetidine hybrids: design, synthesis, in vitro antiproliferative, SAR, in silico molecular docking against VEGFR-2, ADMET, toxicity, and DFT studies," *Bioorganic Chemistry*, vol. 115, Article ID 105206, 2021.

[23] Y. M. Suleimen, A. M. Metwaly, A. E. Mostafa et al., "Isolation, crystal structure, and in silico aromatase inhibition activity of ergosta-5, 22-dien-3β-ol from the fungus gyromitra esculenta," *Journal of Chemistry*, vol. 2021, Article ID 5529786, 10 pages, 2021.

[24] R. G. Yousef, H. M. Sakr, I. H. Eissa et al., "New quinoxaline-2 (1 H)-ones as potential VEGFR-2 inhibitors: design, synthesis, molecular docking, ADMET profile and anti-proliferative evaluations," *New Journal of Chemistry*, vol. 45, no. 36, pp. 16949–16964, 2021.

[25] H. H. Amer, S. H. Alotaibi, A. H. Trawneh, A. M. Metwaly, and I. H. Eissa, "Anticancer activity, spectroscopic and molecular docking of some new synthesized sugar hydrazones, Arylidene and α-Aminophosphonate derivatives," *Arabian Journal of Chemistry*, vol. 14, no. 10, Article ID 103348, 2021.

[26] A. Husain, A. Farooqui, A. Khanam et al., "Physicochemical characterization of C-phycocyanin from Plectonema sp. and elucidation of its bioactive potential through in silico approach," *Cellular and Molecular Biology*, vol. 67, no. 4, pp. 68–82, 2022.

[27] I. H. Eissa, M. M. Khalifa, E. B. Elkaeed, E. E. Hafez, A. A. Alsfouk, and A. M. Metwaly, "In silico exploration of potential natural inhibitors against SARS-Cov-2 nsp10," *Molecules*, vol. 26, no. 20, p. 6151, 2021.

[28] E. B. Elkaeed, I. H. Eissa, A. M. Saleh, B. A. Alsfouk, and A. M. Metwaly, "Computer-aided drug discovery of natural antiviral metabolites as potential SARS-CoV-2 helicase inhibitors," *Journal of Chemical Research*, vol. 48, no. 1, 2024.

[29] E. B. Elkaeed, R. G. Yousef, H. Elkady et al., "New anticancer theobromine derivative targeting EGFR(WT) and EGFR(T790M): design, semi-synthesis, in silico, and in vitro anticancer studies," *Molecules*, vol. 27, no. 18, p. 5859, 2022.

[30] E. B. Elkaeed, I. H. Eissa, H. Elkady et al., "A multistage in silico study of natural potential inhibitors targeting SARS-CoV-2 main protease," *International Journal of Molecular Sciences*, vol. 23, no. 15, p. 8407, 2022.

[31] E. B. Elkaeed, A. M. Metwaly, M. S. Alesawy, A. M. Saleh, A. A. Alsfouk, and I. H. Eissa, "Discovery of potential SARS-CoV-2 papain-like protease natural inhibitors employing a multi-phase in silico approach," *Life*, vol. 12, no. 9, p. 1407, 2022.

[32] I. H. Eissa, M. S. Alesawy, A. M. Saleh et al., "Ligand and structure-based in silico determination of the most promising SARS-CoV-2 nsp16-nsp10 2 o-methyltransferase complex inhibitors among 3009 FDA approved drugs," *Molecules*, vol. 27, no. 7, p. 2287, 2022.

[33] E. B. Elkaeed, H. Elkady, A. Belal et al., "Multi-phase in silico discovery of potential SARS-CoV-2 RNA-dependent RNA polymerase inhibitors among 3009 clinical and FDA-approved related drugs," *Processes*, vol. 10, no. 3, p. 530, 2022.

[34] A. M. Metwaly, A. Elwan, A.-A. M. M. El-Attar, S. T. Al-Rashood, and I. H. Eissa, "Structure-based virtual screening, docking, ADMET, molecular dynamics, and MM-PBSA calculations for the discovery of potential natural SARS-CoV-2 helicase inhibitors from the traditional Chinese medicine," *Journal of Chemistry*, vol. 2022, Article ID 7270094, 23 pages, 2022.

[35] E. B. Elkaeed, B. A. Alsfouk, T. H. Ibrahim et al., "Computer-assisted drug discovery of potential natural inhibitors of the SARS-CoV-2 RNA-dependent RNA polymerase through a multi-phase in silico approach," *Antiviral Therapy*, vol. 28, no. 5, 2023.

[36] A. A. Agbowuro, W. M. Huston, A. B. Gamble, and J. D. Tyndall, "Proteases and protease inhibitors in infectious diseases," *Medicinal Research Reviews*, vol. 38, no. 4, pp. 1295–1331, 2018.

[37] Q.-S. Du, S.-Q. Wang, Y. Zhu et al., "Polyprotein cleavage mechanism of SARS CoV Mpro and chemical modification of the octapeptide," *Peptides*, vol. 25, no. 11, pp. 1857–1864, 2004.

[38] A. Hegyi and J. Ziebuhr, "Conservation of substrate specificities among coronavirus main proteases," *Journal of General Virology*, vol. 83, no. 3, pp. 595–599, 2002.

[39] P.-H. Liang, "Characterization and inhibition of SARS-coronavirus main protease," *Current Topics in Medicinal Chemistry*, vol. 6, no. 4, pp. 361–376, 2006.

[40] S. Ullrich and C. Nitsche, "The SARS-CoV-2 main protease as drug target," *Bioorganic and Medicinal Chemistry Letters*, vol. 30, no. 17, Article ID 127377, 2020.

[41] Fda-approved Drug Library, https://www.selleckchem.com/screening/fda-approved-drug-library.html, 2021.

[42] A. Douangamath, D. Fearon, P. Gehrtz et al., "Crystallographic and electrophilic fragment screening of the SARS-CoV-2 main protease," *Nat Commun*, vol. 11, no. 1, pp. 1–11, 2020.

[43] A. L. Carvalho, J. Trincão, and M. J. J. L. Romão, "protocols," *X-ray Crystallography in Drug Discovery*, Springer, Berlin, Germanypp. 31–56, 2010.

[44] A. M. Hassell, G. An, R. K. Bledsoe et al., "Crystallization of protein–ligand complexes," *Acta Crystallographica Section D Biological Crystallography*, vol. 63, no. 1, pp. 72–79, 2007.

[45] D. Vidal, R. Garcia-Serna, and J. Mestres, "Ligand-based approaches to in silico pharmacology," in *Chemoinformatics and Computational Chemical Biology*, pp. 489–502, Springer, Berlin, Germany, 2011.

[46] G. Schneider, Y. Tanrikulu, and P. Schneider, "Self-organizing Molecular Fingerprints: A Ligand-Based View on Drug-like Chemical Space and Off-Target Prediction," *Future Med Chem*, vol. 1, 2009.

[47] M. A. Spackman and J. J. McKinnon, "Fingerprinting intermolecular interactions in molecular crystals," *CrystEngComm*, vol. 4, no. 66, pp. 378–392, 2002.

[48] H. Chu, Q.-X. He, J. Wang, Y. Hu, Y.-Q. Wang, and Z.-H. Lin, "In silico design of novel benzohydroxamate-based compounds as inhibitors of histone deacetylase 6 based on 3D-QSAR, molecular docking, and molecular dynamics simulations," *New Journal of Chemistry*, vol. 44, no. 48, pp. 21201–21210, 2020.

[49] C. Ieritano, J. L. Campbell, and W. S. Hopkins, "Predicting differential ion mobility behaviour in silico using machine learning," *Analyst*, vol. 146, no. 15, pp. 4737–4743, 2021.

[50] M. Taha, N. H. Ismail, M. Ali et al., "Molecular hybridization conceded exceptionally potent quinolinyl-oxadiazole hybrids through phenyl linked thiosemicarbazide antileishmanial scaffolds: in silico validation and SAR studies," *Bioorganic Chemistry*, vol. 71, pp. 192–200, 2017.

[51] K. Heikamp and J. R. Bajorath, "How do 2D fingerprints detect structurally diverse active compounds? Revealing compound subset-specific fingerprint features through systematic selection," *Journal of Chemical Information and Modeling*, vol. 51, no. 9, pp. 2254–2265, 2011.

[52] F. A. D. M. Opo, M. M. Rahman, F. Ahammad, I. Ahmed, M. A. Bhuiyan, and A. M. Asiri, "Structure based pharmacophore modeling, virtual screening, molecular docking and ADMET approaches for identification of natural anti-cancer agents targeting XIAP protein," *Scientific Reports*, vol. 11, no. 1, pp. 4049–4117, 2021.

[53] J. Duan, S. L. Dixon, J. F. Lowrie, and W. Sherman, "Analysis and comparison of 2D fingerprints: insights into database screening performance using eight fingerprint methods," *Journal of Molecular Graphics and Modelling*, vol. 29, no. 2, pp. 157–170, 2010.

[54] M. Sastry, J. F. Lowrie, S. L. Dixon, and W. Sherman, "Large-scale systematic analysis of 2D fingerprint methods and parameters to improve virtual screening enrichments," *Journal of Chemical Information and Modeling*, vol. 50, no. 5, pp. 771–784, 2010.

[55] T. Kogej, O. Engkvist, N. Blomberg, and S. Muresan, "Multifingerprint based similarity searches for targeted class compound selection," *Journal of Chemical Information and Modeling*, vol. 46, no. 3, pp. 1201–1213, 2006.

[56] P. Willett, "Molecular similarity approaches in chemoinformatics: early history and literature status," *Frontiers in Molecular Design and Chemical Information Science-Herman Skolnik Award Symposium*, ACS Publications, Jürgen Bajorath, 2016.

[57] G. Maggiora, M. Vogt, D. Stumpfe, and J. Bajorath, "Molecular similarity in medicinal chemistry: miniperspective," *Journal of Medicinal Chemistry*, vol. 57, no. 8, pp. 3186–3204, 2014.

[58] T. Altamash, A. Amhamed, S. Aparicio, and M. Atilhan, "Effect of hydrogen bond donors and acceptors on CO2 absorption by deep eutectic solvents," *Processes*, vol. 8, no. 12, p. 1533, 2020.

[59] Y. Wan, Y. Tian, W. Wang, S. Gu, X. Ju, and G. Liu, "In silico studies of diarylpyridine derivatives as novel HIV-1 NNRTIs using docking-based 3D-QSAR, molecular dynamics, and pharmacophore modeling approaches," *RSC Advances*, vol. 8, no. 71, pp. 40529–40543, 2018.

[60] M. Turchi, Q. Cai, and G. Lian, "An evaluation of in-silico methods for predicting solute partition in multiphase complex fluids–A case study of octanol/water partition coefficient," *Chemical Engineering Science*, vol. 197, pp. 150–158, 2019.

[61] K. M. Sullivan, S. J. Enoch, J. Ezendam, K. Sewald, E. L. Roggen, and S. Cochrane, "An adverse outcome pathway for sensitization of the respiratory tract by low-molecular-weight chemicals: building evidence to support the utility of

in vitro and in silico methods in a regulatory context," *Applied In Vitro Toxicology*, vol. 3, no. 3, pp. 213–226, 2017.

[62] A. Escamilla-Gutiérrez, R. M. Ribas-Aparicio, M. G. Córdova-Espinoza, and J. A. Castelán-Vega, "In silico strategies for modeling RNA aptamers and predicting binding sites of their molecular targets," *Nucleosides, Nucleotides and Nucleic Acids*, vol. 40, no. 8, pp. 798–807, 2021.

[63] A. C. Kaushik, A. Kumar, S. Bharadwaj, R. Chaudhary, and S. Sahi, "Ligand-based approach for in-silico drug designing," in *Bioinformatics Techniques for Drug Discovery*, pp. 11–19, Springer, Berlin, Germany, 2018.

[64] H. Zhang, J.-X. Ren, J.-X. Ma, and L. Ding, "Development of an in silico prediction model for chemical-induced urinary tract toxicity by using naïve Bayes classifier," *Molecular Diversity*, vol. 23, no. 2, pp. 381–392, 2019.

[65] R. C. Braga and C. H. Andrade, "Assessing the performance of 3D pharmacophore models in virtual screening: how good are they?" *Current Topics in Medicinal Chemistry*, vol. 13, no. 9, pp. 1127–1138, 2013.

[66] M. Muchtaridi, H. N. Syahidah, A. Subarnas, M. Yusuf, S. D. Bryant, and T. Langer, "Molecular docking and 3D-pharmacophore modeling to study the interactions of chalcone derivatives with estrogen receptor alpha," *Pharmaceuticals*, vol. 10, no. 4, p. 81, 2017.

[67] A. Kutlushina, A. Khakimova, T. Madzhidov, and P. Polishchuk, "Ligand-based pharmacophore modeling using novel 3D pharmacophore signatures," *Molecules*, vol. 23, no. 12, p. 3094, 2018.

[68] A. McGechan and K. Wellington, "Ramelteon," *CNS Drugs*, vol. 19, no. 12, pp. 1057–1065, 2005.

[69] P. K. Yadalam, T. M. Balaji, S. Varadarajan et al., "Assessing the therapeutic potential of agomelatine, ramelteon, and melatonin against SARS-CoV-2," *Saudi Journal of Biological Sciences*, vol. 29, no. 5, pp. 3140–3150, 2022.

[70] P. Krishnamoorthy, A. S. Raj, S. Roy, N. S. Kumar, and H. Kumar, "Comparative transcriptome analysis of SARS-CoV, MERS-CoV, and SARS-CoV-2 to identify potential pathways for drug repurposing," *Computers in Biology and Medicine*, vol. 128, Article ID 104123, 2021.

[71] Y. Chen, H. Tao, S. Shen et al., "A drug screening toolkit based on the–1 ribosomal frameshifting of SARS-CoV-2," *Heliyon*, vol. 6, no. 8, Article ID e04793, 2020.

[72] D. De Amici, F. Ramaioli, P. Ceriana, and E. Percivalle, "Antiviral activity of local anaesthetic agents," *Journal of Antimicrobial Chemotherapy*, vol. 37, no. 3, p. 635, 1996.

[73] M. Hosseini, W. Chen, D. Xiao, and C. Wang, "Computational molecular docking and virtual screening revealed promising SARS-CoV-2 drugs," *Precision clinical medicine*, vol. 4, no. 1, pp. 1–16, 2021.

[74] S. D. Black, "Molecular modeling and preliminary clinical data suggesting antiviral activity for chlorpheniramine (chlorphenamine) against COVID-19," *Cureus*, vol. 14, no. 1, Article ID e20980, 2022.

[75] S. A. Hollingsworth and R. O. Dror, "Molecular dynamics simulation for all," *Neuron*, vol. 99, no. 6, pp. 1129–1143, 2018.

[76] X. Liu, D. Shi, S. Zhou, H. Liu, H. Liu, and X. Yao, "Molecular dynamics simulations and novel drug discovery," *Expert Opinion on Drug Discovery*, vol. 13, no. 1, pp. 23–37, 2018.

[77] Y. X. Zhu, Y. J. Sheng, Y. Q. Ma, and H. M. Ding, "Assessing the performance of screening MM/PBSA in protein-ligand interactions," *Journal of Physical Chemistry*, vol. 126, no. 8, pp. 1700–1708, 2022.

[78] T. Fu, Z. Jin, Z. Xiu, and G. Li, "Binding free energy estimation for protein-ligand complex based on MM-PBSA with various partial charge models," *Current Pharmaceutical Design*, vol. 19, no. 12, pp. 2293–2307, 2013.

[79] G. Poli, C. Granchi, F. Rizzolio, and T. Tuccinardi, "Application of MM-PBSA methods in virtual screening," *Molecules*, vol. 25, no. 8, p. 1971, 2020.

[80] A. M. Metwaly, E. B. Elkaeed, B. A. Alsfouk, A. M. Saleh, A. E. Mostafa, and I. H. Eissa, "The computational preventive potential of the rare flavonoid, patuletin, isolated from Tagetes patula, against SARS-CoV-2," *Plants*, vol. 11, no. 14, p. 1886, 2022.

[81] M. S. Alesawy, E. B. Elkaeed, A. A. Alsfouk, A. M. Metwaly, and I. H. Eissa, "In silico screening of semi-synthesized compounds as potential inhibitors for SARS-CoV-2 papain-like protease: pharmacophoric features, molecular docking, ADMET, toxicity and DFT studies," *Molecules*, vol. 26, no. 21, p. 6593, 2021.

[82] P. D. bank, *R P D Bank*, PD Bank, Jalgaon, India, 2020.

[83] S. Jo, T. Kim, V. G. Iyer, and W. Im, "CHARMM-GUI: a web-based graphical user interface for CHARMM," *Journal of Computational Chemistry*, vol. 29, no. 11, pp. 1859–1865, 2008.

[84] B. R. Brooks, C. L. Brooks III, A. D. Mackerell Jr. et al., "CHARMM: the biomolecular simulation program," *Journal of Computational Chemistry*, vol. 30, no. 10, pp. 1545–1614, 2009.

[85] J. Lee, X. Cheng, J. M. Swails et al., "CHARMM-GUI input generator for NAMD, GROMACS, AMBER, OpenMM, and CHARMM/OpenMM simulations using the CHARMM36 additive force field," *Journal of Chemical Theory and Computation*, vol. 12, no. 1, pp. 405–413, 2016.

[86] R. B. Best, X. Zhu, J. Shim et al., "Optimization of the additive CHARMM all-atom protein force field targeting improved sampling of the backbone ϕ, ψ and side-chain χ_1 and χ_2 dihedral angles," *Journal of Chemical Theory and Computation*, vol. 8, no. 9, pp. 3257–3273, 2012.

[87] J. C. Phillips, R. Braun, W. Wang et al., "Scalable molecular dynamics with NAMD," *Journal of Computational Chemistry*, vol. 26, no. 16, pp. 1781–1802, 2005.